Article

Synthesis and properties of cyclic sandwich compounds

https://doi.org/10.1038/s41586-023-06192-4

Received: 12 October 2022

Accepted: 10 May 2023

Published online: 2 August 2023

Check for updates

Luca Münzfeld[1], Sebastian Gillhuber[1], Adrian Hauser[1], Sergei Lebedkin[2], Pauline Hädinger[1], Nicolai D. Knöfel[1], Christina Zovko[1], Michael T. Gamer[1], Florian Weigend[3], Manfred M. Kappes[2,4] & Peter W. Roesky[1]✉

Cyclic nanometre-scale sandwich complexes assembled from individual building blocks were synthesized. Sandwich complexes, in which a metal ion is π-coordinated by two planar aromatic organic rings belong to the foundations of organometallic chemistry. They have been successfully used in a wide variety of applications ranging from catalysis, synthesis and electrochemistry to nanotechnology, materials science and medicine[1,2]. Extending the sandwich structural motif leads to linear multidecker compounds, in which aromatic organic rings and metal atoms are arranged in an alternating fashion. However, the extension to a cyclic multidecker scaffold is unprecedented. Here we show the design, synthesis and characterization of an isomorphous series of circular sandwich compounds, for which the term 'cyclocenes' is suggested. These cyclocenes consist of 18 repeating units, forming almost ideally circular, closed rings in the solid state, that can be described by the general formula $[cyclo\text{-}M^{II}(\mu\text{-}\eta^8{:}\eta^8\text{-}Cot^{TIPS})]_{18}$ (M = Sr, Sm, Eu; Cot^{TIPS} = 1,4-(^{i}Pr$_3$Si)$_2$C$_8$H$_6^{2-}$). Quantum chemical calculations lead to the conclusion that a unique interplay between the ionic metal-to-ligand bonds, the bulkiness of the ligand system and the energy gain on ring closure, which is crucially influenced by dispersion interactions, facilitate the formation of these cyclic systems. Up to now, only linear one-dimensional multidecker sandwich compounds have been investigated for possible applications such as nanowires[3–10]. This textbook example of cyclic sandwich compounds is expected to open the door for further innovations towards new functional organometallic materials.

The isolation of ferrocene and the explanation of its molecular structure marked the origin of modern organometallic chemistry[11–13]. In the wake of this milestone discovery, sandwich complexes and their derivatives have had an unparalleled impact on the development and theoretical foundations of chemistry itself[1,2]. Sandwich compounds with two cyclopentadienyl ligands (Cp, $C_5H_5^-$) are classically referred to as metallocenes. However, the strict definition of metallocenes is not obligatory in scientific terminology nowadays. Particularly in the case of the *f* elements, compounds with larger ligand systems, such as cyclooctatetraenediide, are also referred to as metallocenes.

The simplest molecular sandwich compounds, $[M(C_nH_n)_2]^{+/0/-}$ (C_nH_n with a π-aromatic ring), can formally be considered to be the smallest entity. The next larger scaffold are triple-decker compounds $[M_2(C_nH_n)_3]^{+/0/-}$ (refs. 14,15). Following this thought, multidecker compounds of the general type $[M_n(C_nH_n)_{n+1}]^{+/0/-}$ can then be considered the next (evolutionary) step of the sandwich complex family. Here, more than two metal ions are complexed by $n-1$ bridging as well as two capping π-perimeter ligands yielding one-dimensional (1D) coordination oligomers. Today, the field of multidecker sandwich compounds is subject to intense research due to their intriguing properties and structural motifs resulting in possible applications such as nanowires[3–10].

The concept of using higher dimensional metal-containing networks or specifically shaped structures is not new to organometallic chemistry[16,17]. However, despite more 70 years of research, sandwich compounds, in which the structure is exclusively assembled by direct metal–ligand interactions, are still limited to simple chains or related motifs[18]. Apart from this, some examples of circular oligomeric metallopolymers based on *ansa*-ferrocene or -ruthenocene derivatives are known. Here, interconnecting frameworks provided by ligand-ligand bonds by means of $SiMe_2$– (refs. 19–21), CHR– (R = H, Me) (refs. 22–24) or C–C bonds have been reported[25]. However, these species do not feature any multidecker structural motifs.

Herein, we showcase the design, synthesis and characterization of an isomorphous series of circular sandwich compounds solely consisting of multiple, equivalent direct metal–ligand interactions. Reminiscent of classical metallocenes, we propose the term 'cyclocenes' for this fundamentally new compound class.

[1]Institute of Inorganic Chemistry, Karlsruhe Institute of Technology (KIT), Karlsruhe, Germany. [2]Institute of Nanotechnology, Karlsruhe Institute of Technology (KIT), Eggenstein-Leopoldshafen, Germany. [3]Department of Chemistry, Philipps University of Marburg, Marburg, Germany. [4]Institute of Physical Chemistry, Karlsruhe Institute of Technology (KIT), Karlsruhe, Germany. ✉e-mail: roesky@kit.edu

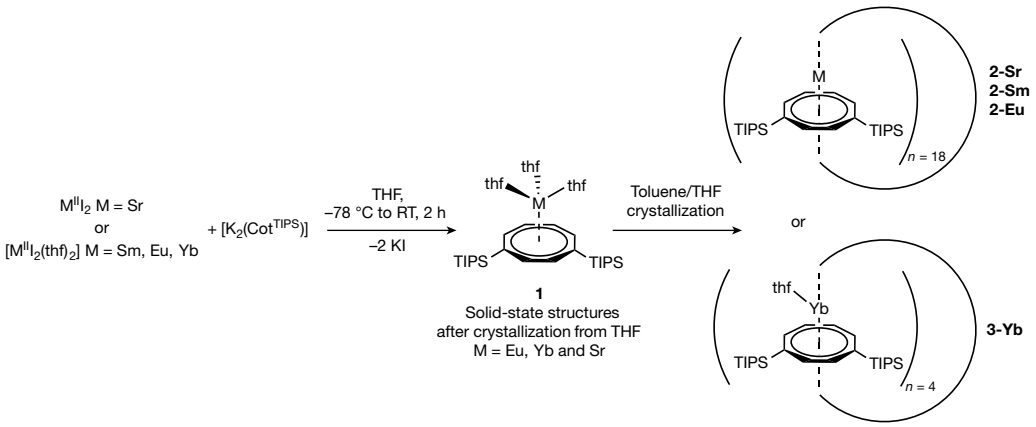

Fig. 1 | Cyclocene synthesis. Synthesis of $[M^{II}(thf)_3(\eta^8\text{-}Cot^{TIPS})]$ (**1**), $[cyclo\text{-}M^{II}(\mu\text{-}\eta^8\text{:}\eta^8\text{-}Cot^{TIPS})]_{18}$ (**2, M = Sr, Sm, Eu**) and $[cyclo\text{-}Yb^{II}(\mu\text{-}\eta^2\text{:}\eta^8\text{-}Cot^{TIPS})(thf)]_4$ (**3-Yb**). RT, room temperature.

Synthesis of cyclic sandwich compounds

In lanthanide chemistry, only 1D-multidecker sandwich-based oligomers could so far be constructed as supramolecular structures. Typical examples are $[M^{II/III}{}_n(Cot)_m]$ polydecker ($Cot = C_8H_8^{2-}$) compounds (M = Sc, Y, La, Ce, Nd, Eu, Tb, Ho, Tm, Yb; up to $n = 30$ for Eu; $m = n$, $n - 1$, $n + 1$), which are commonly prepared by laser evaporation and molecular beam methods and obtained as a mixture of compounds with varying chain lengths[3–7]. Isolation and structural characterization on a preparative scale have not been reported. Another approach is based on the direct reduction of neutral Cot derivatives by elemental lanthanides in liquid ammonia, yielding $[Ln^{II}{}_n(Cot)_m]$ (Ln = Eu, Yb) species[6,26,27]. In the absence of a suitable donor, intermolecular assembly to polymeric 1D-multidecker stacks was claimed[6]. Despite manifold publications describing the physical properties of such multidecker compounds, no solid-state structures have been reported so far.

To form a ring-shaped sandwich compound, n metal ions would require complexation by n π-perimeter ligands to give a closed topology. Two simple prerequisites for a circular sandwich compound can be formulated: (1) a cyclic system would ideally show an overall neutral charge. Thus, a homoleptic system with an equal charge magnitude on the metal centres and ligand moieties appears expedient. (2) A constant bending should be present in each sandwich subunit to construct the target assembly. The $[Ln^{II}{}_n(Cot)_m]$ (Ln = Eu, Yb) polydeckers mentioned above meet the first criterion. Strong evidence that the second prerequisite can also be satisfied was recently reported by our group. We showed that the introduction of bulky Cot derivatives into the samarium quadrupledecker $[Sm^{III/II/III}{}_3(Cot^{TIPS})_4]$ (Cot^{TIPS} = 1,4-($^iPr_3Si$)$_2C_8H_6^{2-}$) induces substantial unidirectional bending. In particular, the divalent subunit of this complex shows a pronounced bent structure with a Ct–Sm–Ct (Ct, ligand centroid) angle accounting for roughly 160° (ref. 28). Assuming that the magnitude and unidirectional character of this bending is retained in an analogue $[Ln^{II}{}_n(Cot^{TIPS})_n]$ complex, a circular system of about 18 units might be formed if only a slight deviation from a 160° bending angle takes place.

Reactions of the divalent alkaline earth and lanthanide iodides $Sr^{II}I_2$ or $[M^{II}I_2(thf)_2]$ (M = Sm, Eu, Yb) with $[K_2(Cot^{TIPS})]$ in tetrahydrofuran (THF) resulted in monomeric THF-solvated $[M^{II}(thf)_3(\eta^8\text{-}Cot^{TIPS})]$ complexes (**1**, M = Sr, Eu, Yb). All complexes tend to lose the coordinated THF molecules rapidly on removing the mother liquor (Fig. 1; further details on this and on the synthesis can be found in the Supplementary Information). The samarium species could not be obtained as crystalline material. The molecular structures in the solid-state of **1** resemble the piano stool motif described previously for the related complex $[Yb^{II}(pyr)_3(\eta^8\text{-}Cot)]$ (pyr, pyridine)[26] (the Supplementary Information gives structural details of **1**). Attempts to fully characterize **1** were unsuccessful because **1-Sr** and **1-Eu** lose all solvent molecules rapidly on drying the isolated crystalline materials. In the case of **1-Yb**, one equivalent of THF is retained. This is a first indication that THF free compounds of the type $[Ln^{II}{}_n(Cot^{TIPS})_n]$ are formed on drying **1-Sr** or **1-Eu**. Consequently, THF coordination must be suppressed during crystallization to allow the formation of oligomeric systems, exclusively containing M^{II}-Cot interactions. However, several crystallization attempts involving non-coordinating solvents, such as toluene or *n*-heptane, exclusively yielded amorphous material. Addition of small amounts of THF to toluene crystallization batches eventually facilitated the isolation of single crystals (Supplementary Information). Single-crystal X-ray diffraction analysis revealed that the metal ions of similar ionic radii Sr^{II}, Sm^{II} and Eu^{II} form cyclo-*octadeca*-sandwich complexes $[cyclo\text{-}M^{II}(\mu\text{-}\eta^8\text{:}\eta^8\text{-}Cot^{TIPS})]_{18}$ (**2**, Fig. 2).

The M–Ct distances are similar throughout the series and show only slight variations within the corresponding cyclocene (**2-Sr** 2.209(2)–2.263(1) Å, **2-Sm** 2.189(1)–2.2518(11) Å, **2-Eu** 2.1783(7)–2.2276(7) Å). All Ct–M–Ct angles show values marginally above the postulated 160°. This is caused by the ring plane being slightly puckered (**2-Sr** 160.85(6)–166.11(7)°, **2-Sm** 161.61(6)–165.13(6)°, **2-Eu** 161.89(4)–165.27(4)°). Likewise, all M–M–M angles are of a similar magnitude (**2-Sr** 157.36(4)–163.46(4)°, **2-Sm** 157.36(3)–161.83(3)°, **2-Eu** 157.52(2)–161.40(2)°), with inner angle sums close to 360° (**2-Sr** 366.04°, **2-Sm** 363.12°, **2-Eu** 364.61°), resulting in almost ideally circular structures, with a slight elliptical deformation. The inner diameters of the ring systems account for roughly 17 Å, whereas the outer diameters amount to roughly 38 Å (Supplementary Tables 9–11).

By contrast, by using the smaller Yb^{II} ion a formal cyclo-*tetra*-ytterbocen $[cyclo\text{-}Yb^{II}(\mu\text{-}\eta^2\text{:}\eta^8\text{-}Cot^{TIPS})(thf)]_4$ (**3-Yb**, Fig. 2, bottom right) was obtained in which the open face of the Yb^{II} coordination sphere is saturated by one THF ligand. We assume that the κ^1-THF-Yb^{II} bonds are strengthened compared to Sr^{II}, Sm^{II} and Eu^{II} due to the higher Lewis acidity of Yb^{II}. Thus, the contracted motif is favoured over a cyclo-*octadeca*-sandwich structure (see below for quantum chemical calculations).

To probe the structural composition of compounds **2** in solution, diffusion ordered nuclear magnetic resonance spectroscopy (DOSY-NMR) experiments were performed on the diamagnetic complex **2-Sr** and the paramagnetic complex **2-Eu**. In THF-d_8, these experiments yielded hydrodynamic radii of R_h = 6.9 Å (**2-Sr**) and 5.3 Å (**2-Eu**), indicative of monomeric species of the type $[M^{II}(thf)_3(\eta^8\text{-}Cot^{TIPS})]$ (**1**) being present. In the non-coordinating solvent toluene-d_8 the hydrodynamic radii account for R_h = 5.3 Å (**2-Sr**) and 5.0 Å (**2-Eu**) (Supplementary Information). Although a comparison of DOSY measurements in different solvents should be considered with caution, these values significantly deviate from what would be expected if the cyclo-*octadeca*-sandwich structures were retained in solution. Consequently, the cyclic motif is

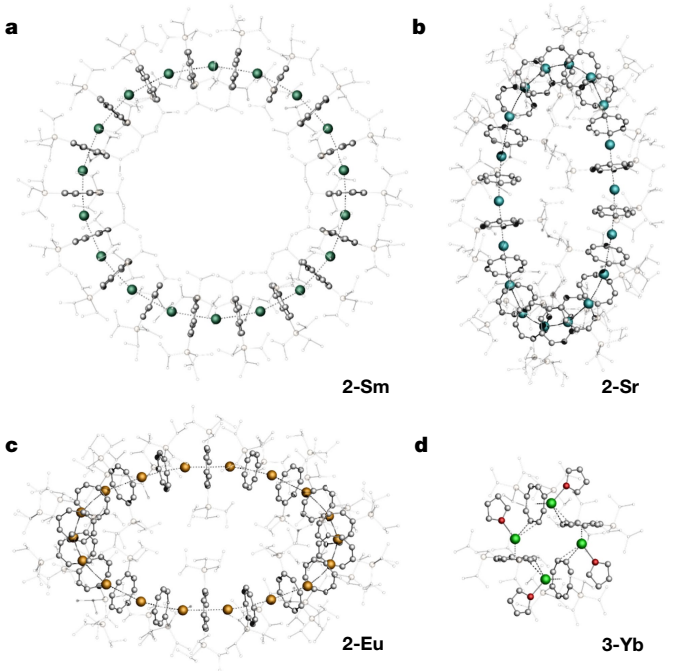

Fig. 2 | Cyclocene structures. a, Molecular structures in the solid state of [*cyclo*-Sm^{II}(μ-η^8:η^8-COT^{TIPS})]$_{18}$ (**2-Sm**). **b**, [*cyclo*-Sr^{II}(μ-η^8:η^8-Cot^{TIPS})]$_{18}$ (**2-Sr**). **c**, [*cyclo*-Eu^{II}(μ-η^8:η^8-Cot^{TIPS})]$_{18}$ (**2-Eu**). **d**, [*cyclo*-Yb^{II}(μ-η^2:η^8-Cot^{TIPS})(thf)]$_4$ (**3-Yb**). Hydrogen atoms are omitted, and Si^{i}Pr$_3$-groups are shown transparently for better clarity. Note that the cyclo-*octadeca*-sandwich complexes [*cyclo*-M^{II}(μ-η^8:η^8-Cot^{TIPS})]$_{18}$ **2-Sm, 2-Sr** and **2-Eu** are depicted from different perspectives for improved visualization of the circular structures. However, they are isostructural.

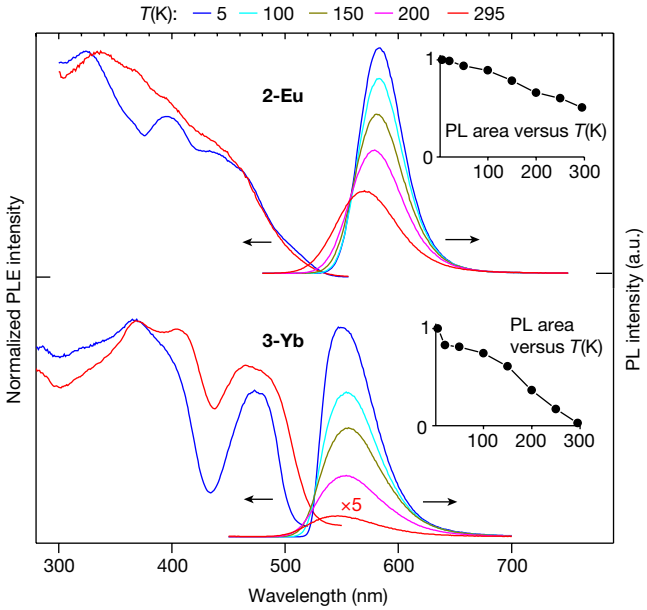

Fig. 3 | Photoluminescence properties. Excitation (PLE) and emission spectra of **2-Eu** and **3-Yb** in solid (polycrystalline) state at different temperatures between 5 and 295 K. The PLE and PL spectra were recorded and excited at 580 and 350 (**2-Eu**), and 550 and 350 nm (**3-Yb**), respectively. The inserts show the integral emission intensity (normalized to unity) as a function of temperature.

most probably formed by means of self-assembly pathways on crystallization. Similarly, plumbocene [Pb(Cp)$_2$][29,30] can form different chains or a hexameric cyclic scaffold with Pb-η^5-Cp-Pb bridges, depending on the crystallization conditions. However, the lead atom is coordinated by three η^5-Cp-rings and thus does not resemble a classical sandwich motif.

Photoluminescence properties

The solid cyclocenes **2-Eu** and **3-Yb** demonstrate orange and green photoluminescence (PL) centred at 570 and 546 nm, respectively, which slightly redshifts to 583 and 550 nm at cryogenic temperatures (Fig. 3). The excitation onset at about 520 nm corresponds to the visual appearance of the samples as yellow (**2-Eu**) or yellow-greenish (**3-Yb**) polycrystalline powders, as well as to their absorption spectra (Supplementary Fig. 33, note that the PL excitation (PLE) and absorption spectra overemphasize the intensity of weak bands due to a high optical thickness of the sample preparations and non-validity of the Beer–Lambert law). The emission of **2-Eu** occurs with a high quantum efficiency of Φ_{PL} = 60% at room temperature (estimated as approaching 100% at 5 K) and decays monoexponentially on ns-pulsed laser excitation at 337 nm with τ = 2.1/1.7 µs at 5/295 K (Supplementary Fig. 31). Accordingly, it shows only a moderate temperature dependence. A similar PL has been observed for other complexes of divalent europium, including sandwich compounds, and can be assigned to a $4f^6 5d^1 \rightarrow 4f^7$ transition of the Eu^{2+} ions in **2-Eu** (refs. 6,31). The low-energy absorption or PLE bands also relate to the *f*–*d* transitions of Eu^{2+} as no contribution of molecular orbitals of the Cot^{TIPS} ligands is expected above roughly 400 nm absorption or PL excitation wavelength[32]. The energies of emissive *f*–*d* transitions of divalent europium and ytterbium in related compounds are typically comparable. In consistence, the emissions of **2-Eu** and **3-Yb** are close spectrally (Fig. 3)[33].

Other PL properties differ, however, notably, reflecting in part the different complexation patterns discussed above. In contrast to **2-Eu**, the PL intensity and kinetics of **3-Yb** show a strong temperature dependence. The PL of the latter is relatively weak at ambient temperature, but increases roughly 40-fold on cooling, with Φ_{PL} rising from 1.0% at 295 K to about 37% at 5 K as estimated from the emission spectra. The PL decay is clearly non-monoexponential within the whole temperature interval probed. The effective (average) decay time derived from biexponential fits varies from 0.78 µs at room temperature to 23 µs at 170 K and 220 µs at 5 K (Supplementary Fig. 32). A large radiative lifetime (roughly 600 and 80 µs at 5 and 295 K) indicates a spin-forbidden $4f^{13}5d^1 \rightarrow 4f^{14}$ emissive transition in **3-Yb**. Its efficient non-radiative quenching is probably contributed to by the presence of THF molecules in the coordination sphere (Fig. 3) and their vibrational coupling to the Yb^{2+} ions. This might also explain the different temperature effects on the absorption onset seen in the excitation spectra (note to Supplementary Fig. 33).

Quantum chemical calculations

For a more detailed understanding of the ring formation, density functional theory calculations were performed using TURBOMOLE[34,35].

Table 1 | Calculated Ct–M–Ct angles

	[M$^{II}_3$Cot$_4$]$^{2-}$	[M$^{II}_3$Cot$^{TMS}_4$]$^{2-}$	[M$^{II}_3$Cot$^{TIPS}_4$]$^{2-}$	[*cyclo*-M^{II}(μ-η^8:η^8-Cot^{TIPS})]$_{18}$ (2)[a]
Sr	179.7°	178.2°	161.6°	163.1°
Sm	179.3°	178.0°	163.2°	163.4°
Eu	179.7°	177.5°	161.8°	163.5°

Ct–M–Ct angles of the central ring-metal-ring motif of [M$^{II}_3$(Cot$^{(TMS/TIPS)}$)$_4$]$^{2-}$ units (M=Sm, Eu, Sr). Geometries were optimized at level PBE0/def2-TZVP/D4/COSMO, that is, using the hybrid density functional by Perdew, Burke, and Ernzerhof, PBE0, error-balanced polarized triple-zeta valence basis sets, def2-TZVP, the D4 dispersion correction, and the conductor-like screening model, COSMO (references can be found in the Supplementary Information). [a]Average value calculated from the nine unique Ct–M–Ct angles of the corresponding solid-state structure.

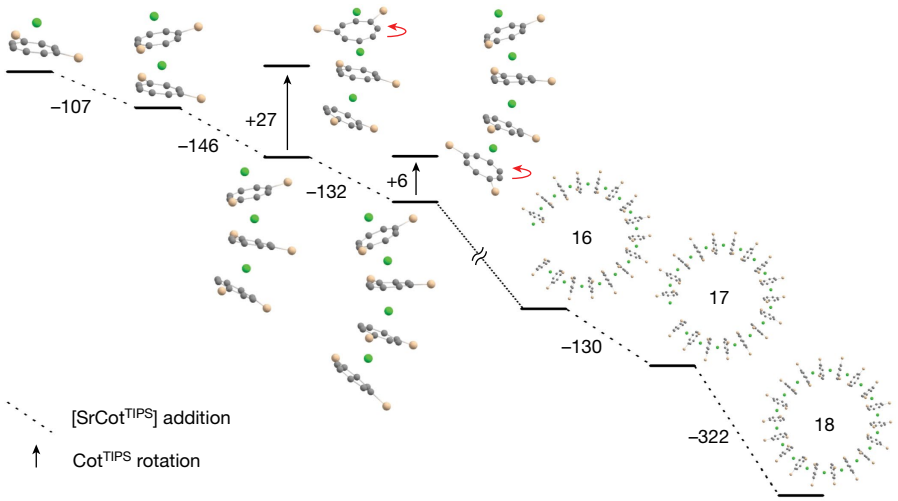

Fig. 4 | Quantum chemical calculations. Sr-based model systems to investigate the difference between the formation of a cyclic and chain-type structure. H atoms and ^{i}Pr groups are omitted for clarity. Sr is drawn in green, Si in beige, C in grey. Given energies (in kJ mol^{-1}) refer to single-point calculations at the PBE0/def2-TZVP/D4 level of theory for structures optimized at the PBE/SV(P)/D4 level. Further details and computational settings are given within the Supplementary Information.

Details are given within the Supplementary Information, and optimized structures of all compounds in the appendix of the Supplementary Information.

At first, the bonding situation in the new class of sandwich complexes was investigated. For this, the smallest unit, namely [M^{II}(Cot^{TIPS})] (M = Sr, Sm, Eu, Yb), was extracted from the cyclocene structure, and its electronic properties were investigated. The bonding between the metal ions and the Cot^{TIPS} units in the cyclocenes is predominantly of electrostatic nature. This is evident from the absence of significant covalent interactions, as visible, for example, from Foster–Boys localization[36], which did not yield any orbital with noteworthy contributions of both the metal and any of the ring carbons.

In fact, natural population analysis[37] charges of the metal ions amount to 1.76/1.27/1.28/1.26 elementary charges for M = Sr, Sm, Eu, Yb (Supplementary Table 12), similar to analogue charges for metal halides of the type M^{II}X$_2$ (M = Sr, Sm, Eu, Yb; X = Cl, Br, I), which are classically considered ionic compounds containing divalent metal ions (Supplementary Table 14). Also, the absence of *s* valence electrons at the metal ions (from the same analysis, Supplementary Table 12) in the [M^{II}(Cot^{TIPS})] fragments is in accordance with chemical intuition. Explicitly including scalar-relativistic effects and spin-orbit coupling does not change this picture. Virtually the same results were obtained for the larger fragments [M$^{II}_3$(Cot^{TIPS})$_4$]$^{2-}$ (for M = Sr, Sm, Eu) considered below (Supplementary Table 13).

The pronounced bending observed in the cyclocene structures is due to steric reasons, which becomes evident when studying the Ct–M–Ct bending angle for a section of the ring consisting of three metal ions and four ring moieties using substituents with different steric demands. In detail, the steric demand of the ring substituents was varied from H ([M$^{II}_3$(Cot)$_4$]$^{2-}$) to TMS (TMS is trimethylsilane, Me$_3$Si) ([M$^{II}_3$(Cot^{TMS})$_4$]$^{2-}$, Cot^{TMS} = 1,4-(Me$_3$Si)$_2$C$_8$H$_6^{2-}$) to TIPS ([M$^{II}_3$(Cot^{TIPS})$_4$]$^{2-}$). The Ct–M–Ct angle of the central ring-M-ring unit is shown in Table 1. For Cot, a linear arrangement with a Ct–M–Ct angle close to 180° is found, allowing for the formation of polymeric 1D stacks as outlined above. When TMS groups are introduced, a bending is induced, leading to Ct–M–Ct angles of roughly 178°. The transition to the more sterically demanding TIPS groups leads to a more pronounced bending with Ct–M–Ct angles of 161–163°, in good agreement with the experimentally obtained values, thereby allowing for the formation of 18-membered ring structures. This indicates that the cyclocene size might be tailored by modifying the bulk of the Cot substituents[38].

Obviously, the steric demand of the substituents is responsible for the bending of the individual ring-M-ring units. However, this sterically induced bending leads to the formation of the observed cyclic structures only when it occurs in a unidirectional manner. Otherwise, the formation of chain-type structures is also conceivable. The difference between these two options was investigated by considering the Sr model systems partially depicted in Fig. 4. Relevant energy differences based on these structures are given in Supplementary Tables 15 and 16. The following picture emerges from the calculations: (1) arrangements representing sections of the ring molecule are energetically preferred by 6 to 27 kJ mol^{-1} over the lowest energy arrangement unsuitable for ring formation. (2) The energy gain for ring formation is about 140 kJ mol^{-1}, estimated from the reaction energy of [Sr(Cot^{TIPS})]$_{n-1}$ + [Sr(Cot^{TIPS})] → [Sr(Cot^{TIPS})]$_n$ for n = 2 to n = 17. For the ring closure (n = 18), it is more than twice as large, 322 kJ mol^{-1}. (3) Dispersion interactions are only slightly larger (2–16 kJ mol^{-1}) for arrangements suitable for ring formation than for unsuitable arrangements. However, dispersion interactions make up more than half of the reaction energy, making them crucial for stabilizing the structures.

To summarize, the ability to form a ring is due to the specific design of the Cot^{TIPS} ligand, but the driving force for the ring formation is the energy gained by its closure, which is missing when a non-cyclic structural motif is formed.

Finally, we rationalized the formation of a four-membered ring in case of Yb, contrary to the formation of 18-membered rings for Sr, Sm and Eu. As discussed above, cyclocene formation is mainly determined by two factors, namely ionic interactions between the metal atom and the Cot derivative as well as its steric demand. Whereas the latter is the same for all Cot^{TIPS} compounds, the ionic radius of Yb^{II} (1.14 Å) differs significantly from that of Sr^{II} (1.26 Å), Sm^{II} (1.27 Å) and Eu^{II} (1.25 Å) (coordination number 8). This in turn reveals that the observed structural differences are apparently induced by the smaller ionic radius of Yb^{II} compared to Sr^{II}, Sm^{II} and Eu^{II} (ref. 39). The extra nuclear charge of Yb (Z = 70) compared to Sm (Z = 62) and Eu (Z = 63) is only weakly shielded by the extra *f* electrons, leading to a significant increase in the effective nuclear charge Z_{eff} and thus a decrease in the ionic radius. A smaller ionic radius indicates two consequences that are relevant here: (1) the Lewis acidity of Yb^{II} is increased relative to Sr^{II}, Sm^{II} and Eu^{II}, leading to a higher tendency to form Lewis acid–base adducts when a Lewis base is present. This is evidenced, for instance, by the fact that the solvates **1** readily lose all solvent ligands on drying in vacuo in the case of **1-Sr**

and **1-Eu**, whereas for **1-Yb** one equivalent of THF is retained. In fact, the calculated binding energy of THF to [$M^{II}(Cot^{TIPS})$] (M = Sr, Sm, Eu, Yb) fragments is about 15 kJ mol^{-1} higher for Yb^{II} than for the other metals (Supplementary Table 17). (2) The ligands in a sandwich complex show smaller M-ring distances, in line with smaller inter-ring distances, leading to increased steric repulsion between two ring ligands. This, together with the presence of an extra THF prevents the formation of an 18-membered ring structure for Yb and rationalizes the formation of a smaller ring.

Conclusion

The isolation and structural characterization of the cyclocene family [*cyclo*-$M^{II}(\mu\text{-}\eta^8\text{:}\eta^8\text{-}Cot^{TIPS})]_{18}$ (M = Sr, Sm, Eu) opens a fundamental, new chapter in the chemistry of sandwich compounds. The formation of these fascinating species has been rationalized aided by quantum chemical methods and translated into basic design principles towards future ventures into the synthesis of cyclocenes. The pronounced bending observed in the cyclocene structures is caused by the steric demand of the Cot substituents. The driving force for the ring formation is the energy gained by its closure, which is largely influenced by dispersion interactions, and missing when a non-cyclic structural motif is formed. The stability and size of cyclocenes is assumed to be adjustable by specifically tailoring the used ligand systems. Considering this prospect in the light of classical sandwich compounds and their well-established properties, this textbook example of the cyclocene motif is expected to find further application in functional organometallic chemistry.

Online content

Any methods, additional references, Nature Portfolio reporting summaries, source data, extended data, supplementary information, acknowledgements, peer review information; details of author contributions and competing interests; and statements of data and code availability are available at https://doi.org/10.1038/s41586-023-06192-4.

1. Togni, A. *Metallocenes: Synthesis, Reactivity, Applications* (Wiley-VCH, 1998).
2. Štěpnička, P. *Ferrocenes: Ligands, Materials and Biomolecules* (John Wiley & Sons, Ltd, 2008).
3. Miyajima, K., Knickelbein, M. B. & Nakajima, A. Stern–Gerlach study of multidecker lanthanide–cyclooctatetraene sandwich clusters. *J. Phys. Chem. A.* **112**, 366–375 (2008).
4. Hosoya, N. et al. Lanthanide organometallic sandwich nanowires: formation mechanism. *J. Phys. Chem. A.* **109**, 9–12 (2005).
5. Kurikawa, T. et al. Multiple-decker sandwich complexes of lanthanide-1,3,5,7-cyclooctatetraene [$Ln_n(C_8H_8)_m$] (Ln=Ce, Nd, Eu, Ho, and Yb); localized ionic bonding structure. *J. Am. Chem. Soc.* **120**, 11766–11772 (1998).
6. Tsuji, T. et al. Liquid-phase synthesis of multidecker organoeuropium sandwich complexes and their physical properties. *J. Phys. Chem. C.* **118**, 5896–5907 (2014).
7. Huttmann, F., Schleheck, N., Atodiresei, N. & Michely, T. On-surface synthesis of sandwich molecular nanowires on graphene. *J. Am. Chem. Soc.* **139**, 9895–9900 (2017).
8. Hosoya, N. et al. Formation and electronic structures of organoeuropium sandwich nanowires. *J. Phys. Chem. A* **118**, 8298–8308 (2014).
9. Miyajima, K., Nakajima, A., Yabushita, S., Knickelbein, M. B. & Kaya, K. Ferromagnetism in one-dimensional vanadium–benzene sandwich clusters. *J. Am. Chem. Soc.* **126**, 13202–13203 (2004).
10. Xiang, H., Yang, J., Hou, J. G. & Zhu, Q. One-dimensional transition metal–benzene sandwich polymers: possible ideal conductors for spin transport. *J. Am. Chem. Soc.* **128**, 2310–2314 (2006).
11. Kealy, T. J. & Pauson, P. L. A new type of organo-iron compound. *Nature* **168**, 1039–1040 (1951).
12. Fischer, E. O. & Pfab, W. Cyclopentadien-Metallkomplexe, ein neuer Typ metallorganischer Verbindungen. *Z. Naturforsch., B: Chem. Sci.* **7**, 377–379 (1952).
13. Wilkinson, G., Rosenblum, M., Whiting, M. C. & Woodward, R. B. The structure of iron *bis*-cyclopentadienyl. *J. Am. Chem. Soc.* **74**, 2125–2126 (1952).
14. Werner, H. & Salzer, A. Die Synthese Eines Ersten Doppel-Sandwich-Komplexes: Das Dinickeltricyclopentadienyl-Kation. *Synth. React. Inorg. Met.-Org. Chem.* **2**, 239–248 (1972).
15. Elschenbroich, C. *Organometallics* (Wiley-VCH, 2008).
16. Zhuo, H.-C., Long, J. R. & Yaghi, O. M. Introduction to metal–organic frameworks. *Chem. Rev.* **112**, 673–674 (2012).
17. Kreno, L. E. et al. Metal–organic framework materials as chemical sensors. *Chem. Rev.* **112**, 1105–1125 (2012).
18. Edelmann, F. T. Multiple-decker sandwich complexes of *f*-elements. *New J. Chem.* **35**, 517–528 (2011).
19. Grossmann, B. et al. Seven doubly bridged ferrocene units in a cycle. *Angew. Chem. Int. Ed.* **36**, 387–389 (1997).
20. Herbert, D. E. et al. Redox-active metallomacrocycles and cyclic metallopolymers: photocontrolled ring-opening oligomerization and polymerization of silicon-bridged [1] ferrocenophanes using substitutionally-labile Lewis bases as initiators. *J. Am. Chem. Soc.* **131**, 14958–14968 (2009).
21. Chan, W. Y., Lough, A. J. & Manners, I. Organometallic macrocycles and cyclic polymers by the bipyridine-initiated photolytic ring opening of a silicon-bridged [1]ferrocenophane. *Angew. Chem. Int. Ed.* **46**, 9069–9072 (2007).
22. Watts, W. E. The [1,1]ferrocenophane system 1. *J. Am. Chem. Soc.* **88**, 855–856 (1966).
23. Katz, T. J., Acton, N. & Martin, G. [1n]Ferrocenophanes. *J. Am. Chem. Soc.* **91**, 2804–2805 (1969).
24. Mueller-Westerhoff, U. T. & Swiegers, G. F. A synthesis of the cyclic ferrocene tetramer [1]4ferrocenophane. *Chem. Lett.* **23**, 67–68 (1994).
25. Inkpen, M. S. et al. Oligomeric ferrocene rings. *Nat. Chem.* **8**, 825–830 (2016).
26. Wayda, A. L., Mukerji, I., Dye, J. L. & Rogers, R. D. Divalent lanthanoid synthesis in liquid ammonia. 2. The synthesis and X-ray crystal structure of $(C_8H_8)Yb(C_5H_5N)_3.1/2C_5H_5N$. *Organometallics* **6**, 1328–1332 (1987).
27. Hayes, R. G. & Thomas, J. L. Synthesis of cyclooctatetraenyleuropium and cyclooctatetraenylytterbium. *J. Am. Chem. Soc.* **91**, 6876–6876 (1969).
28. Münzfeld, L., Hauser, A., Hädinger, P., Weigend, F. & Roesky, P. W. The archetypal homoleptic lanthanide quadruple-decker—synthesis, mechanistic studies, and quantum chemical investigations. *Angew. Chem. Int. Ed.* **60**, 24493–24499 (2021).
29. Overby, J. S., Hanusa, T. P. & Young, V. G. Redetermination of the zigzag modification of plumbocene at 173 K. *Inorg. Chem.* **37**, 163–165 (1998).
30. Morrison, C. A., Wright, D. S. & Layfield, R. A. Interpreting molecular crystal disorder in plumbocene, $Pb(C_5H_5)_2$: insight from theory. *J. Am. Chem. Soc.* **124**, 6775–6780 (2002).
31. Suta, M., Kühling, M., Liebing, P., Edelmann, F. T. & Wickleder, C. Photoluminescence properties of the 'bent sandwich-like' compounds $[Eu(Tp^{iPr2})_2]$ and $[Yb(Tp^{iPr2})_2]$ – intermediates between nitride-based phosphors and metallocenes. *J. Lumin.* **187**, 62–68 (2017).
32. Sztainbuch, I. W., Soos, Z. G. & Spiro, T. G. Herzberg–Teller coupling and configuration interaction in a metalloporphyrin model: 1,3,5,7-tetramethylcyclo-octatetraene dianion. *J. Chem. Phys.* **101**, 4644–4648 (1994).
33. Dorenbos, P. Anomalous luminescence of Eu^{2+} and Yb^{2+} in inorganic compounds. *J. Phys. Condens. Matter* **15**, 2645–2665 (2003).
34. TURBOMOLE v.7.6 (University of Karlsruhe and Forschungszentrum Karlsruhe, 1989–2007).
35. Balasubramani, S. G. et al. TURBOMOLE: modular program suite for ab initio quantum-chemical and condensed-matter simulations. *J. Chem. Phys.* **152**, 184107 (2020).
36. Foster, J. M. & Boys, S. F. Canonical configurational interaction procedure. *Rev. Mod. Phys.* **32**, 300–302 (1960).
37. Reed, A. E., Weinstock, R. B. & Weinhold, F. Natural population analysis. *J. Chem. Phys.* **83**, 735–746 (1985).
38. Schneider, E. K., Weis, P., Münzfeld, L., Roesky, P. W. & Kappes, M. M. Anionic stacks of alkali-interlinked yttrium and dysprosium bicyclooctatetraenes in isolation. *J. Am. Soc. Mass. Spectrom.* **33**, 695–703 (2022).
39. Shannon, R. Revised effective ionic radii and systematic studies of interatomic distances in halides and chalcogenides. *Acta Crystallogr., Sect. A.* **32**, 751–767 (1976).

Methods

Synthetic method

Experiments were carried out under a dry, oxygen-free argon atmosphere using Schlenk-line and glovebox techniques. All solvents and reagents were rigorously dried and deoxygenated before use. All compounds were characterized by single-crystal X-ray diffraction studies. Further details are available in the Supplementary Information.

Accession codes

The X-ray crystallographic coordinates for structures reported in this article have been deposited at the Cambridge Crystallographic Data Centre (CCDC), under deposition nos. CCDC 2194266 (**2-Eu**), 2194267 (**2-Sm**), 2194268 (**2-Sr**) and 2194309 (**1-Eu**), 2194310 (**1-Sr**) and 2194311 (**1-Yb**).

Data availability

All data are available in the main text or in the supplementary material. Correspondence and request for materials should be addressed to P.W.R.

Code availability

The TURBOMOLE quantum chemistry program suite is available from https://www.turbomole.org. Calculations were done on a cluster consisting of 8 PCs with 24 Intel(R) Xeon(R) Gold 6212U CPUs each.

Acknowledgements C. Anson, M. Bodensteiner and F. Meurer are acknowledged for discussions about single-crystal X-ray diffraction data refinement. M. Dahlen is acknowledged for supporting PL measurements. Funding was provided by Fonds der Chemischen Industrie, Kekulé fellowship (grant no. 110160). We acknowledge support from the Deutsche Forschungsgemeinschaft (DFG, German Research Foundation) through the Collaborative Research Centre '4f for Future' (CRC 1573 project no. 471424360, projects C1 and Q).

Author contributions Experimental work was carried out by L.M. with support from A.H., P.H. and S.G. PL measurements were carried out by S.L. Single-crystal X-ray diffraction experiments and refinement were done by M.T.G. and L.M. DOSY-NMR was done by N.D.K. and C.Z. Density functional theory calculations were performed by S.G. and F.W. Project administration was done by P.W.R. Supervision was the responsibility of F.W., M.M.K. and P.W.R.

Competing interests The authors declare no competing interests.

Additional information
Supplementary information The online version contains supplementary material available at https://doi.org/10.1038/s41586-023-06192-4.
Correspondence and requests for materials should be addressed to Peter W. Roesky.
Peer review information *Nature* thanks Conrad Goodwin, Andre Schafer and the other, anonymous, reviewer(s) for their contribution to the peer review of this work. Peer reviewer reports are available.